Mechanism-based thermomechanical fatigue life prediction of cast iron. Part II: Comparison of model predictions with experiments

T. Seifert[a,*], G. Maier[a], A. Uihlein[b], K.-H. Lang[b], H. Riedel[a]

[a] *Fraunhofer Institute for Mechanics of Materials IWM, Wöhlerstraße 11, 79108 Freiburg, Germany*
[b] *Universität Karlsruhe (TH), Institut für Werkstoffkunde I, Kaiserstraße 12, 76131 Karlsruhe, Germany*

Abstract

In the present paper, predictions of mechanism-based models for cast iron are compared to experimental results obtained for the nodular cast iron EN-GJS-700, the vermicular cast iron EN-GJV-450 and the lamellar cast iron EN-GJL-250. A strategy is proposed to efficiently identify the model parameters based on isothermal experiments. In particular, complex low cycle fatigue (LCF) tests, tension tests and compression tests are used to adjust the time and temperature dependent cyclic plasticity model. The time and temperature dependent fatigue life prediction model is adjusted to LCF tests. For all investigated cast iron materials, good predictions of thermomechanical fatigue (TMF) tests are possible with the models. Additionally, the location of failure and fatigue life of a thermomechanically loaded double-sided notched specimen are predicted with high accuracy.

Key words: thermomechanical fatigue, life prediction, experimental data, cast iron

1. Introduction

High temperature components in combustion engines must withstand severe cyclic mechanical and thermal loads throughout their life cycle. Espe-

*Corresponding author.
Email addresses: thomas.seifert@iwm.fraunhofer.de (T. Seifert)

cially cylinder heads are often made of cast iron materials, where nodular, vermicular as well as lamellar cast iron is used. The materials undergo low cycle fatigue (LCF) and thermomechanical fatigue (TMF). Thus, reliable methods are necessary to find the appropriate design and material that ensure the integrity of the component for a whole product life at the customer.

It was the aim of a German research project funded by the FVV (Research Association for Combustion Engines) to develop computational methods for fatigue life prediction of high temperature components made of cast iron materials [1]. The methods should allow a substantial reduction of the number of bench tests. To this end, three cast iron materials, namely the nodular cast iron EN-GJS-700, the vermicular cast iron EN-GJV-450 and the lamellar cast iron EN-GJL-250, were tested experimentally at the Institut für Werkstoffkunde I (iwkI) of the Universität Karlsruhe (TH). The experimental results were used at the Fraunhofer Institute for Mechanics of Materials IWM to develop a methodology for calculating the lifetime of thermomechanically loaded components.

In a foregoing paper (Part I: Models), mechanism-based models are developed to describe the time and temperature dependent cyclic plasticity and damage of cast iron materials. The cast iron plasticity model is a combination of the Chaboche model [2, 3, 4], which describes the time and temperature dependent response to cyclic loading, and the Gurson model [5], which describes the effect of the porosity caused by the graphite particles. Thus, the model can describe creep, relaxation and the Bauschinger-effect as well as the tension-compression asymmetry often observed for cast iron. The adjustable parameters of the model are compiled in table 1. On the one hand, the model contains adjustable temperature dependent parameters that quantify time dependency (viscosity) and plasticity of the material. The viscosity parameters are the reference stress K and the exponent n. The plasticity parameters are the initial yield stress σ_Y and parameters of the evolution laws of both backstresses (superscript 1 and 2), which describe kinematic hardening. On the other hand, the model contains constant parameters that are related with porosity: f_N is the volume fraction of the graphite inclusions. s_N is the standard deviation of the nucleation law controlling the tension-compression asymmetry and ε_N and σ_N are mean values, respectively. f_0, f_C and f_F are the initial porosity, the critical porosity for void coalescence and the porosity at failure, respectively.

The fatigue life prediction model is based on the crack-tip blunting model [6, 7]. It assumes that the increment in crack advance per loading cycle is

viscosity:	K, n
plasticity:	σ_Y, C^1, γ_0^1, γ_∞^1, ω^1, R^1, C^2, γ_0^2, γ_∞^2, ω^2, R^2
porosity:	f_N, s_N, ε_N, σ_N, f_0, f_C, f_F

Table 1: Adjustable parameters of the cast iron plasticity model developed in Part I (Models).

of the order of the cyclic crack-tip opening displacement, i.e. $da/dN = \beta \Delta CTOD$. The factor β implicitly depends on the volume fraction f_N of the graphite inclusions and other microstructural quantities characterizing the graphite morphology. An analytical estimate of $\Delta CTOD$ is used which results in the damage parameter D_{TMF} [8]. D_{TMF} contains the parameters compiled in table 2. The cyclic yield stress σ_{CY} and the Ramberg-Osgood hardening exponent N can be determined from the saturated stress-strain hysteresis loop of the isothermal fatigue experiments. Approximate values for the Norton exponent m are frequently known from literature. These parameters depend on temperature. Q is the activation energy for creep and α is an adjustable parameter.

plasticity:	σ_{CY}, N
creep:	m, Q, α

Table 2: Parameters of the damage parameter D_{TMF} presented in Part I (Models).

The damage parameter is correlated with the number of cycles to failure, $N_f = A/\left(D_{TMF}\right)^B$. A and B are introduced as adjustable parameters. The values $A = 2\ln\left[a_f/a_0\right]/\beta \approx 8/\beta$ and $B = 1$ are predicted from the underlying theory. a_0 is the initial crack length and a_f the crack length at fracture.

The adjustable parameters of the models must be determined on the basis of experimental data. This data must contain information about all phenomena the models can describe, so that meaningful parameters can be identified [9]. Typically several experiments are carried out like cyclic tests, tensile tests with different strain rates and creep and/or relaxation tests [10, 11]. Therefore, the generation of an experimental basis for the identification of the material parameters can be an expensive issue. A complex LCF loading history is proposed in [12], that allows for the identification of the temperature dependent parameters of viscoplastic models from a small number of specimens. The loading history includes different strain rates, different strain amplitudes and hold times in tension and compression. Stability and sensitivity analyses testify a high quality of the parameters identified from the complex loading program. Moreover, it is possible to predict the material deformation in non-isothermal tests with the identified parameters.

The increasing number of parameters to be determined in the models led to the application of optimization methods, which solve a least-square type problem (e.g. [9, 13, 14, 15, 16]). Gradient-based optimization methods were used e.g. in [17, 9, 13, 18, 19]. Gradient-based methods are effective concerning the necessary function evaluations for finding a minimum. However, appropriate initial values need to be specified to find at least a good local minimum. A strategy to find initial guesses in case of the complex LCF loading history is proposed in [20].

This paper presents a strategy to determine the parameters of the models developed in Part I and comparisons of model prediction with experiments for three cast iron materials. The paper is structured as follows: First, the materials and the experimental procedure are introduced. Then, the strategy and parameter identification procedure is introduced, before the model adjustments to the different cast iron materials are presented. This paper shows only a selection of representative results. A detailed description of all results can be found in the the final report of the research project [1]. The models for EN-GJS-700 are applied to a double-sided notched specimen. Finally, the results are discussed and conclusions are drawn. A list of all symbols used is given in Part I.

2. Experimental

2.1. Materials

Three cast iron materials are considered in this work. The materials were provided by the companies MTU Friedrichshafen (EN-GJS-700), MAN Nürnberg (EN-GJV-450) and Ford (EN-GJL-250) and were taken out of cylinder heads. The chemical compositions of the cast iron materials, determined by spark emission spectroscopy, are given in table 3.

Figure 1 illustrates micrographs of the materials. The cast iron with nodular graphite, EN-GJS-700, has a nearly perlitic matrix. EN-GJV-450 shows a ferritic-perlitic matrix. Besides vermicular graphite, also nodular graphite particles are found. EN-GJL-250 shows a purely perlitic matrix with embedded lamellar graphite particles.

	C	Si	Mn	P	S	Cr	Ni
EN-GJS-700	3.870	1.800	0.510	0.030	0.003	0.860	0.949
EN-GJV-450	3.550	2.190	0.410	0.220	0.010	0.034	0.036
EN-GJL-250	3.460	2.030	0.650	0.030	0.100	0.244	0.116
	Mo	Cu	Al	Ti	V	Nb	W
EN-GJS-700	0.010	0.870	0.007	0.008	0.009	0.005	< 0.005
EN-GJV-450	0.021	0.878	0.003	0.003	0.009	< 0.001	< 0.005
EN-GJL-250	0.019	0.350	0.002	0.024	0.013	0.002	< 0.005

Table 3: Chemical composition of the cast iron materials.

2.2. Experimental setup and procedure

The cast iron materials were tested in air under axial strain control, employing a Schenk servo-hydraulic system of 100 kN dynamic load capacity. Axial strain was measured and controlled with a capacitive extensometer. The specimens were inductively heated using a 5 kW generator and the temperature was measured and controlled by a ribbon Ni-CrNi thermocouple element, positioned in the middle of the gauge length.

Tension and compression tests with a strain rate of 10^{-4} 1/s were conducted for all materials. Furthermore, strain controlled relaxation experiments were performed at elevated temperatures $\theta > 350$ °C. The maximum strain was applied within one second.

2.2.1. Tests with smooth specimens

Solid round specimens were machined with a cylindrical gauge length of 17 mm and a gauge diameter of 7 mm.

Tests with a complex LCF loading history according to figure 2 were performed [12]. The complex loading history consists of different strain rates (10^{-5} 1/s and 10^{-3} 1/s) and hold times in tension (1800 s) and compression (1800 s). In the loading history of figure 2a the strain amplitude is 0.003, while in the loading history of figure 2b different strain amplitudes (0.003 and 0.005) are used. With this complex loading program strain rate effects, stress relaxation and the cyclic hardening properties of the material can be investigated in a single experiment and sufficient information is generated for the determination of the parameters of a time dependent cyclic plasticity model [12]. Additionally, strain controlled LCF tests with a fully reversed strain amplitude were performed at 5 Hz sinusoidal waveform.

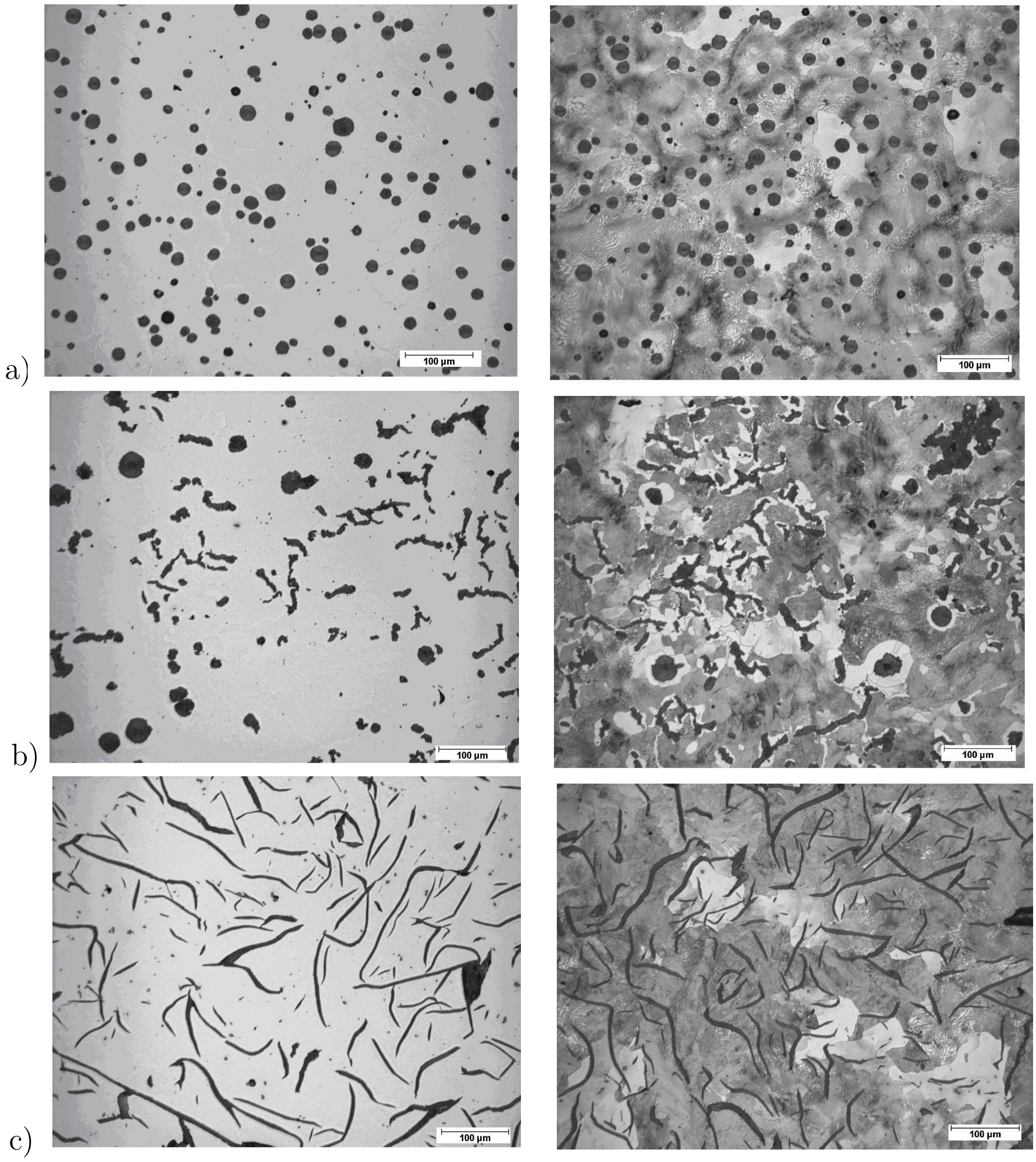

Figure 1: Microstructure of a) EN-GJS-700, b) EN-GJV-450, c) EN-GJL-250; left: unetched, right: etched

The LCF tests were complemented by out-of-phase TMF tests on smooth specimens, in which cyclic thermal loads were applied to specimens with totally suppressed thermal strains. In all experiments the minimum tempera-

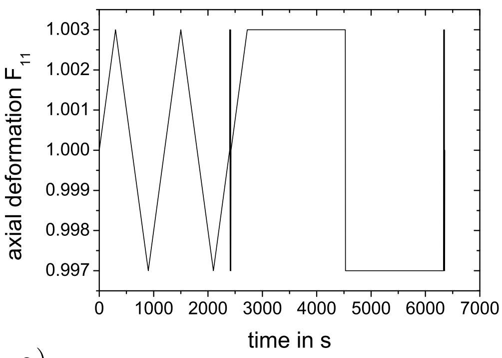

a)

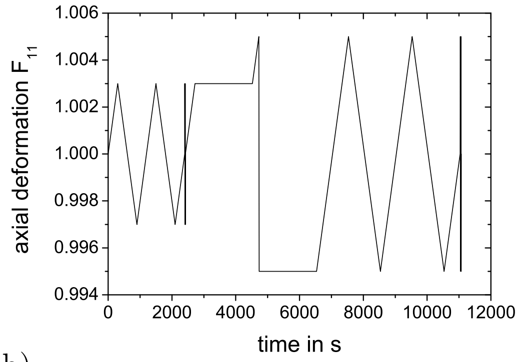

b)

Figure 2: Strain-controlled loading history, consisting of different strain rates (10^{-5} 1/s and 10^{-3} 1/s) and hold times in tension (1800 s) and compression (1800 s). In the loading history a) the strain amplitude is 0.003, while in the loading history b) different strain amplitudes (0.003 and 0.005) are used.

ture was 50 °C and maximum temperatures of 350, 400, 425, 450 or 475 °C were applied. Specimen cooling was mainly achieved by thermal conduction into the specimen grips and could be forced by blowing compressed air on the specimens surface. In all experiments specimens are allowed to expand freely during the initial heating from room temperature up to test temperature. After reaching the testing temperature, a hold time of 60 s secured a stable temperature distribution within the gauge length before the actual experiment was started.

2.2.2. Tests with double-sided notched specimens

Three identical TMF tests were conducted with double-sided notched specimens (figure 3). The geometry of the specimen approximately represents the situation at the I/O valve of a cylinder head. The geometrical dimensions of the specimen were defined such that the notch radius is equal to the width of the ligament. The notch radius is 4 mm.

The thermal strain was totally suppressed between the indentations visible in figure 3. The specimen is heated by induction and the temperature is cycled between 50 and 400 °C. The transient temperature fields were measured by a thermo-camera. Figure 4 shows a thermo-camera image at maximal temperature and the measured temperatures at three different positions upon the specimen during the thermo-cycle. The temperature distribution inside the gauge length is nearly homogeneous.

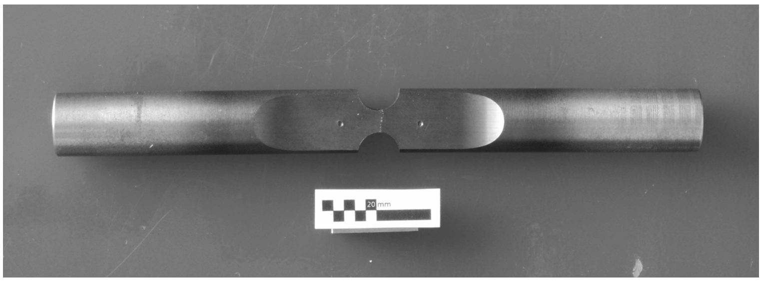

Figure 3: Double-sided notched specimen of EN-GJS-700.

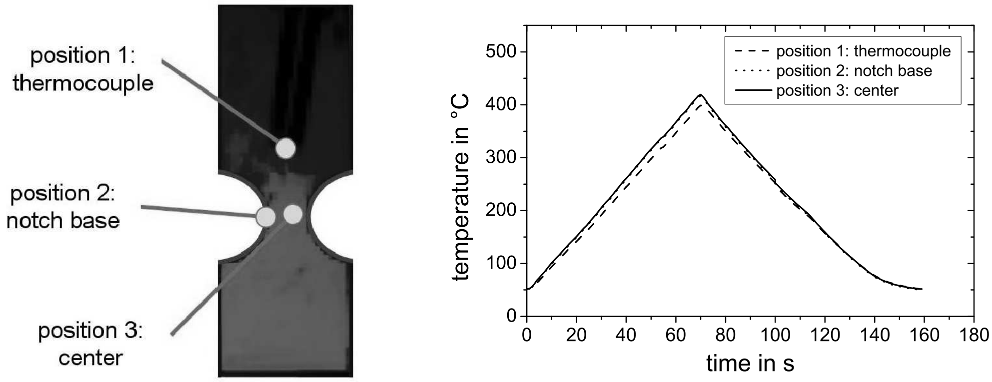

Figure 4: Thermo-camera image of the specimen and resulting temperature-time curves.

3. Parameter identification strategy and procedure

All model parameters are determined on the basis of the results of the tests with smooth specimens (section 2.2.1).

Young's modulus E is determined directly from the first LCF cycle in a range where elastic deformations dominate and verified with the stress-strain hysteresis loop at half lifetime. Poisson's ratio is fixed to 0.3. The thermal expansion coefficients α^{th} are determined from the initial stress-free thermo-cycle of the TMF tests.

The parameters of the cast iron cyclic plasticity model (table 1) are determined on the basis of isothermal experimental data in two steps:

- Step 1: The compressive part of the complex LCF tests and the compression tests are used for the adjustment of the viscosity and plasticity parameters. A fully dense material is assumed in this step. A automated procedure is used considering a least-square minimization problem. The minimization problem is solved using the gradient-based Levenberg-Marquardt method in the form described in [22]. The gradients are computed analytically [20].

- Step 2: The viscosity and plasticity parameters remain unchanged and the porosity parameters are determined such that the data of the tensile tests and the tensile parts of the complex LCF tests, where the effect of the graphite inclusions becomes apparent, is described well.

In order to validate the adjusted parameters using the non-isothermal TMF tests, the model parameters obtained from the isothermal LCF tests are interpolated linearly in temperature.

The parameters of the fatigue life model (table 2) are also determined on the basis of isothermal tests in two steps.

- Step 1: The cyclic yield stress σ_{CY} and the Ramberg-Osgood hardening exponent N are determined from the saturated stress-strain hysteresis loop of the isothermal LCF experiments. To this end, the Ramberg-Osgood relation

$$\delta\varepsilon = \frac{\delta\sigma}{E} + 0.002\,(\sigma_{CY})^{-\frac{1}{N}}\,(\delta\sigma)^{\frac{1}{N}} \tag{1}$$

  is adjusted to the rising branch of the hysteresis. $\delta\varepsilon$ and $\delta\sigma$ are the variations with respect to the lower point of load reversal.

- Step 2: The activation energy for creep Q and the parameter α are identified by adjusting the predicted number of cycles to failure to the measured number of cycles to failure. In this step, also the parameters A and B are determined, relating D_{TMF} to the number of cycles to failure.

Norton's exponent m is fixed to typical values between 3.5 and 4, since no creep tests were performed on the cast materials investigated in this work and no values were found in literature.

4. Model adjustment to EN-GJS-700

4.1. Cast iron plasticity model

The model is adjusted to tests with EN-GJS-700 at 20, 200, 300, 350, 400, 450 and 500 °C. Since the tension/compression asymmetry occurs at larger strains, the strain controlled nucleation law (equation 11 in Part I) is used. The determined porosity parameters are given in table 4.

f_N	s_N	ε_N	f_0	f_C	f_F
0.04	0.001	0	0.02	0.0325	0.25

Table 4: Adjusted porosity parameters for EN-GJS-700.

For some selected tests, the calculated and experimentally measured curves are compared in figure 5 for monotonic tests, in figure 6 for the complex cyclic loading history and in figure 7 for the relaxation tests.

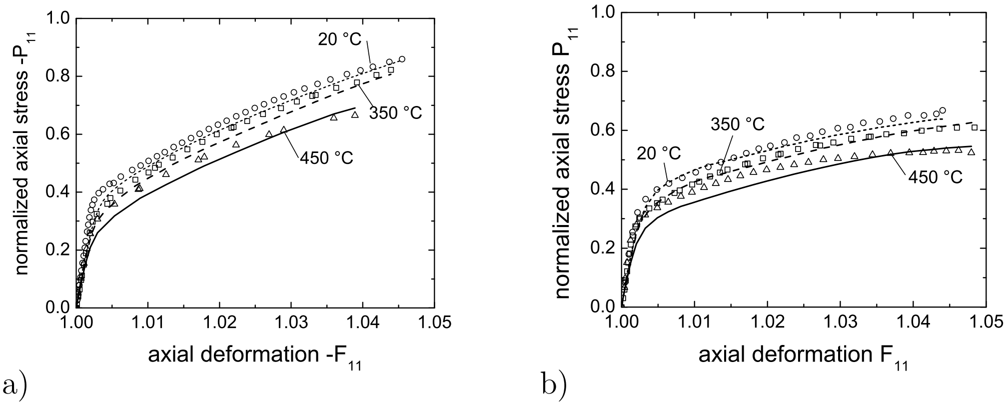

Figure 5: Stress-strain curves of a) compression tests and b) tensile tests for EN-GJS-700. Experimental data is represented by symbols, model response by lines.

Finally, the model predictions for the TMF tests with different temperature ranges are shown in figure 8. A slight modification of the thermal expansion coefficients by about a factor of 1.1 (mod. α^{th} in figure 8) yields an improved description of the data.

4.2. D_{TMF} fatigue life model

The lifetime model is adjusted to the isothermal LCF tests and the fatigue lives of the TMF tests are predicted. The measured numbers of cycles to failure are plotted against the D_{TMF} parameter in figure 9. The cycles to failure fall in a scatter band with factor two compared to the measured cycles to failure, except for 200 °C with $\varepsilon_a = 0.003$. The slope of the fitted line corresponds to the expected value $B = 1$. $A = 25.7$ is determined.

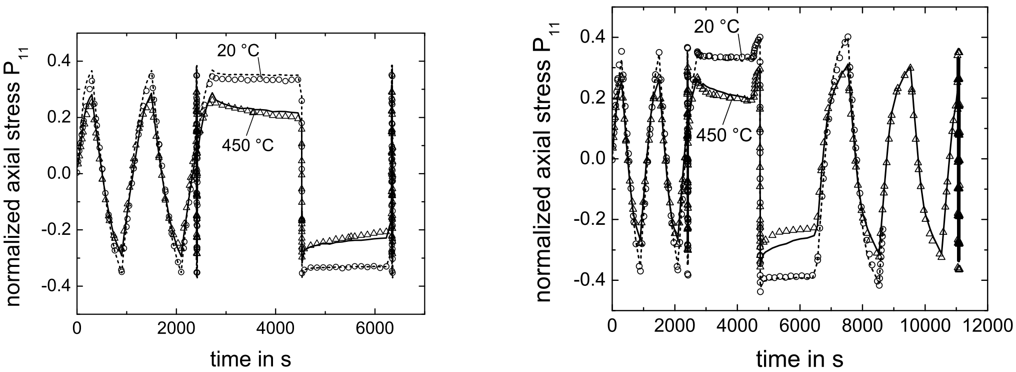

a) b)

Figure 6: Stress-time curves of complex cyclic tests for EN-GJS-700 according to a) figure 2a) and b) figure 2b). Experimental data is represented by symbols, model response by lines.

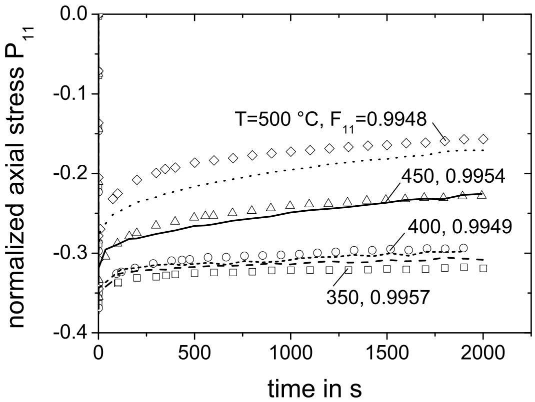

Figure 7: Stress-time curves of relaxation tests at different temperatures for EN-GJS-700. Experimental data is represented by symbols, model response by lines.

5. Model adjustment to EN-GJV-450

5.1. Cast iron plasticity model

The model is adjusted to tests with EN-GJV-450 at 20, 200, 350, 400, 450 and 500 °C. As for EN-GJS-700, the strain controlled nucleation law (equation 11 in Part I) is used. The determined porosity parameters are given in table 5.

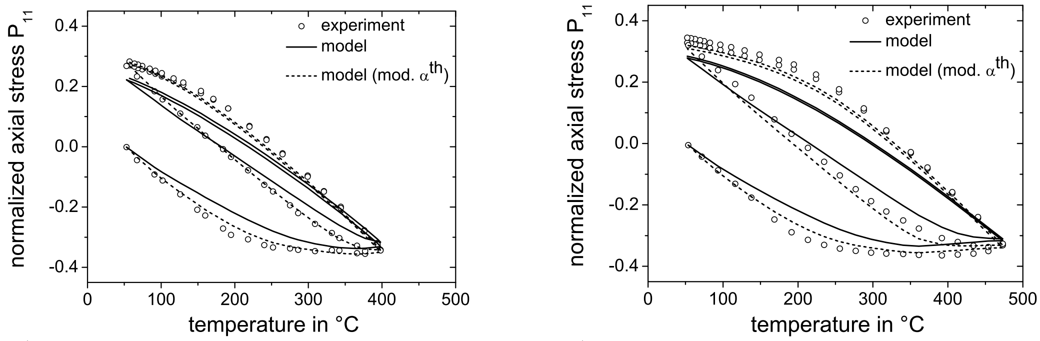

a) b)

Figure 8: Stress-temperature hysteresis loops of TMF tests on smooth specimens for EN-GJS-700. Experimental data is represented by symbols, model response by lines.

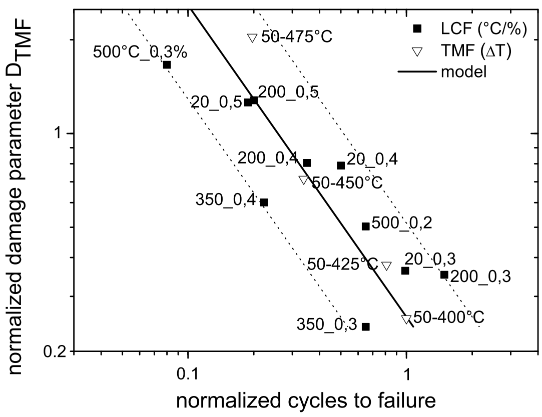

Figure 9: Measured cycles to failure and lifetime model prediction for the LCF and TMF tests with EN-GJS-700. The solid symbols represent the LCF tests with the temperature and applied strain amplitude indicated at the respective symbol. The open symbols represent the TMF tests with the temperature range indicated. The slope of the line has the expected value −1, i.e. $B = 1$.

f_N	s_N	ε_N	f_0	f_C	f_F
0.1	0.001	0	0.05	0.08	0.4

Table 5: Adjusted porosity parameters for EN-GJV-450.

For some selected tests, the calculated and experimentally measured curves are compared in figure 10 for monotonic tests, in figure 11 for the complex cyclic loading history and in figure 12 for the relaxation tests.

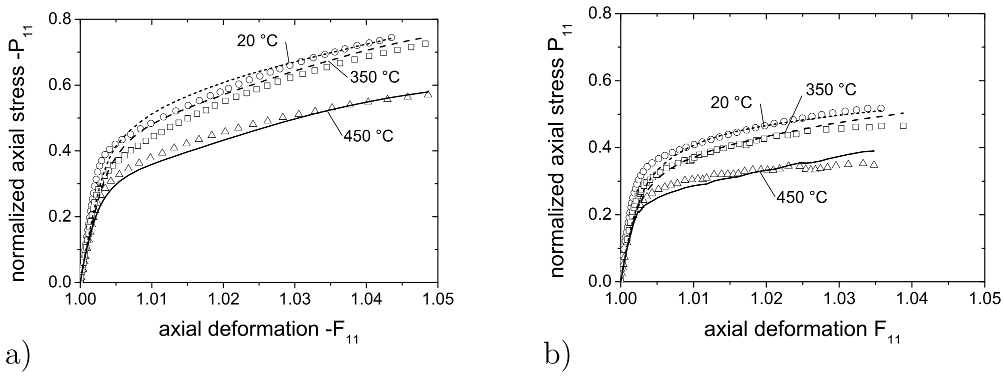

Figure 10: Stress-strain curves of a) compression tests and b) tensile tests for EN-GJV-450. Experimental data is represented by symbols, model response by lines.

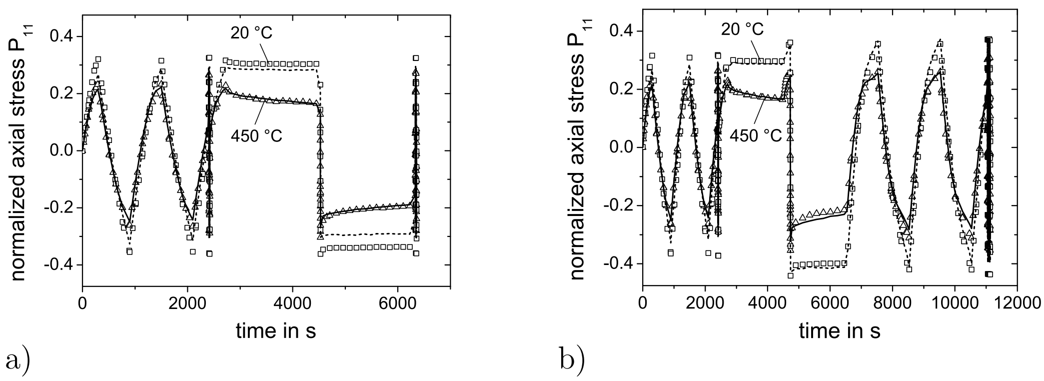

Figure 11: Stress-time curves of complex cyclic tests for EN-GJV-450 according to a) figure 2a) and b) figure 2b). Experimental data is represented by symbols, model response by lines.

Finally, the model predictions for the TMF tests with different temperature ranges are shown in figure 13.

5.2. D_{TMF} fatigue life model

The lifetime model is adjusted to the isothermal LCF tests and the fatigue lives of TMF experiments are predicted. The measured numbers of cycles to

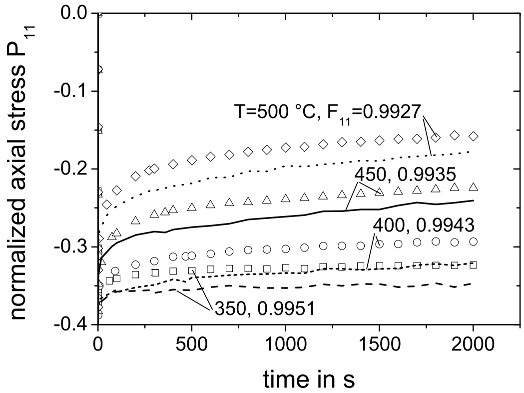

Figure 12: Stress-time curves of relaxation tests at different temperatures for EN-GJV-450. Experimental data is represented by symbols, model response by lines.

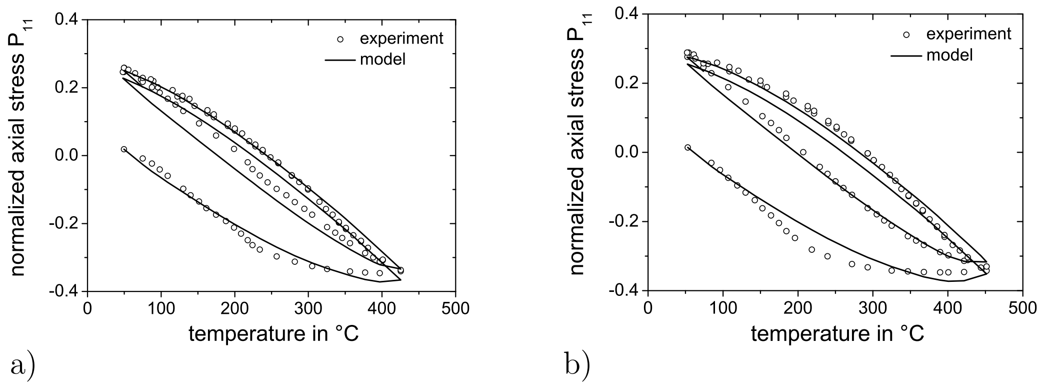

Figure 13: Stress-temperature hysteresis loops of TMF tests on smooth specimens for EN-GJV-450. Experimental data is represented by symbols, model response by lines.

failure are plotted against the D_{TMF} parameter in figure 14. The cycles to failure fall in a scatter band with factor of slightly greater than two compared to the measured values. The slope of the fitted line corresponds to $B = 1$, and $A = 9.91$ is found.

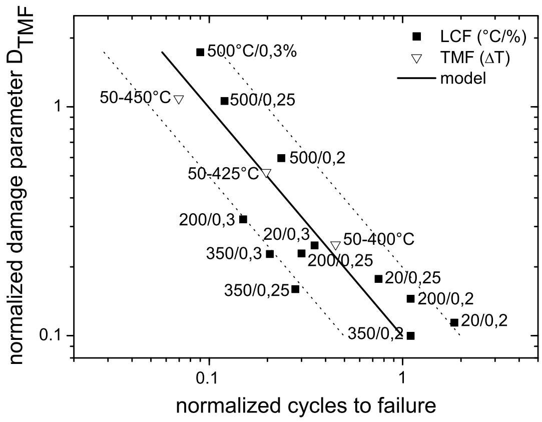

Figure 14: Measured cycles to failure and lifetime model prediction for the LCF and TMF tests with EN-GJV-450. The solid symbols represent the LCF tests with the temperature and applied strain amplitude indicated at the respective symbol. The open symbols represent the TMF tests with the temperature range indicated. The slope of the line has the expected value −1, i.e. $B = 1$.

6. Model adjustment to EN-GJL-250

6.1. Cast iron plasticity model

The model is adjusted to tests with EN-GJL-250 at 20, 200, 300, 350, 400 and 450 °C. Since the tension/compression asymmetry occurs for EN-GJL-250 already at small strains, the stress controlled nucleation law (equation 12 in Part I) is used. The determined porosity parameters are given in table 6.

f_N	s_N in MPa	σ_N in MPa	f_0	f_C	f_F
0.25	50	−30	0.125	1	1

Table 6: Adjusted porosity parameters for EN-GJL-250.

For some selected tests, the calculated and experimentally measured curves are compared in figure 15 for monotonic tests, in figure 16 for the complex cyclic loading history and in figure 17 for the relaxation tests.

Finally, the model predictions for the TMF tests with different temperature ranges are shown in figure 18. A slight modification of the thermal expansion coefficients by about a factor of 1.1 (mod. α^{th} in figure 18) yields an improved description of the data.

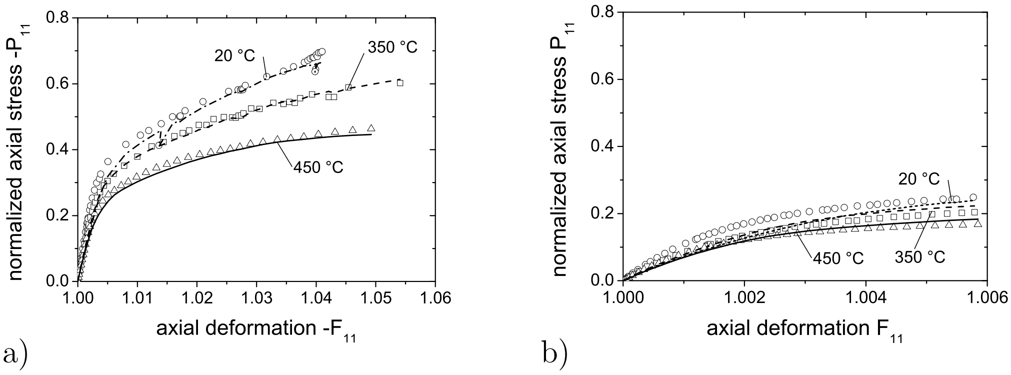

Figure 15: Stress-strain curves of a) compression tests and b) tensile tests for EN-GJL-250. Experimental data is represented by symbols, model response by lines.

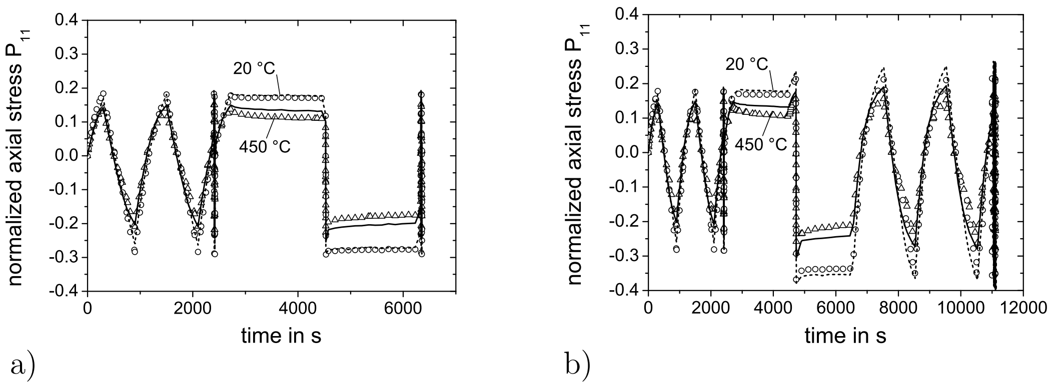

Figure 16: Stress-time curves of complex cyclic tests for EN-GJL-250 according to a) figure 2a) and b) figure 2b). Experimental data is represented by symbols, model response by lines.

6.2. D_{TMF} fatigue life model

The lifetime model is adjusted to the isothermal LCF tests and the fatigue lives of TMF experiments are predicted. The measured numbers of cycles to failure are plotted against D_{TMF} in figure 19. Most of the tests fall within the scatter band with factor two. Scattering is typically more pronounced for lamellar cast iron. The slope of the fitted line corresponds to $B = 1$. $A = 2.71$ is determined.

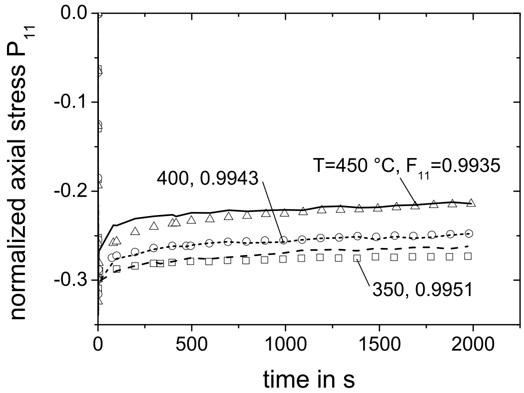

Figure 17: Stress-time curves of relaxation tests at different temperatures for EN-GJL-250. Experimental data is represented by symbols, model response by lines.

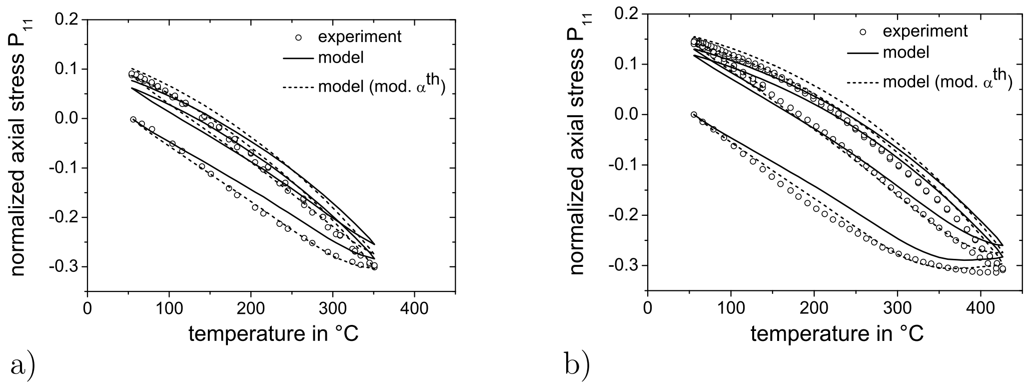

Figure 18: Stress-temperature hysteresis loops of TMF tests on smooth specimens for EN-GJL-250. Experimental data is represented by symbols, model response by lines.

7. TMF life prediction of the double-sided notched specimen

The methodology for TMF life prediction, developed in Part I and adjusted to various cast iron materials is applied to predict the fatigue life of the double-sided notched specimens made of EN-GJS-700. The fatigue life is predicted via finite-element calculations. To this end, the models for cast iron were implemented into the finite-element program ABAQUS/Standard [23] using the implicit algorithms described in [20, 21]. Some remarks on the finite-element implementation are given in Part I. The calculations assume

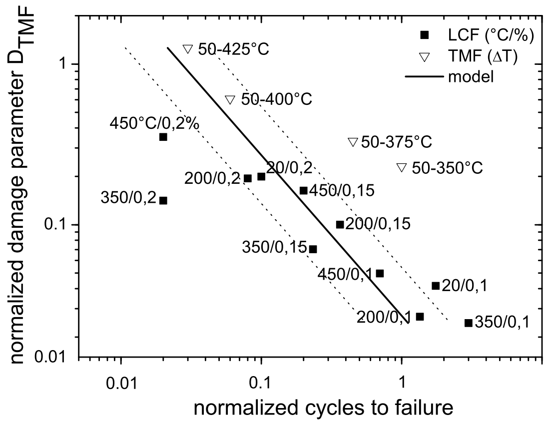

Figure 19: Measured cycles to failure and lifetime model prediction for the LCF and TMF tests with EN-GJL-250. The solid symbols represent the LCF tests with the temperature and applied strain amplitude indicated at the respective symbol. The open symbols represent the TMF tests with the temperature range indicated. The slope of the line has the expected value -1, i.e. $B = 1$.

a homogeneous temperature distribution. The temperature history at the center of the specimen (position 3 in figure 4) is used. Due to symmetry, only one eighth of the specimen is modeled.

Figure 20 shows the calculated number of cycles to failure. The critical location is the center of the notch where 949 cycles to failures are predicted. This corresponds very well to the measured number of cycles to failure, which is 821 ± 253 cycles for three tests. The location of failure also matches well with experimental observations: crack initiation always occurred in the center of the notch with an approximately semi-circular crack shape (figure 21).

8. Discussion

In Part I mechanism-based models are developed that describe the essential features of the time and temperature dependent cyclic plasticity and fatigue damage of cast iron materials. In this paper, a strategy is proposed to determine the model parameters. The strategy is used to adjust the models to experimental data of the cast iron materials EN-GJS-700, EN-GJV-450 and EN-GJL-250.

The model for the time and temperature dependent cyclic plasticity of cast iron, a combination of the Chaboche model and the Gurson model, is

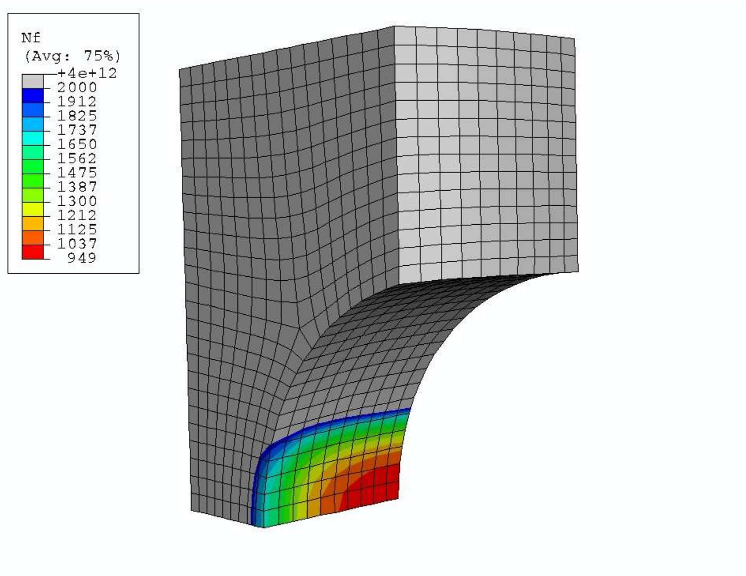

Figure 20: Predicted fatigue lives of the double-sided notched specimen made of EN-GJS-700.

adjusted to the isothermal tests, namely the complex LCF tests and the tension and compression tests. For all materials, the model describes several aspects of the material behavior well: (1) the stress level decreases with increasing temperature, (2) time dependent effects become more pronounced with increasing temperature and (3) the tension-compression asymmetry, which is apparent already at small strains for EN-GJL-250, while it does not appear before larger strains are attained for the other materials. With the parameters adjusted with the proposed procedure, a good description of the TMF tests is obtained. The description is improved by slightly modifying the coefficients of thermal expansion. Such a variation is acceptable since the coefficients frequently exhibit considerable scatter in these materials.

For the nodular cast iron EN-GJS-700, the porosity achievable by nucleation alone is obtained from the parameter fit as $f_N = 0.04$. This is consistent with the graphite volume fraction in this material. For the lamellar cast iron EN-GJL-250, however, the graphite volume fraction is highly overestimated with the value $f_N = 0.25$. Supposedly, the discrepancy in caused by the fact that the Chaboche-Gurson model is based on spherical inclusions, whereas the graphite inclusions are lamellar. The model could be improved by using the model of Gologanu et al. [24, 25] instead of the Gurson model, so that

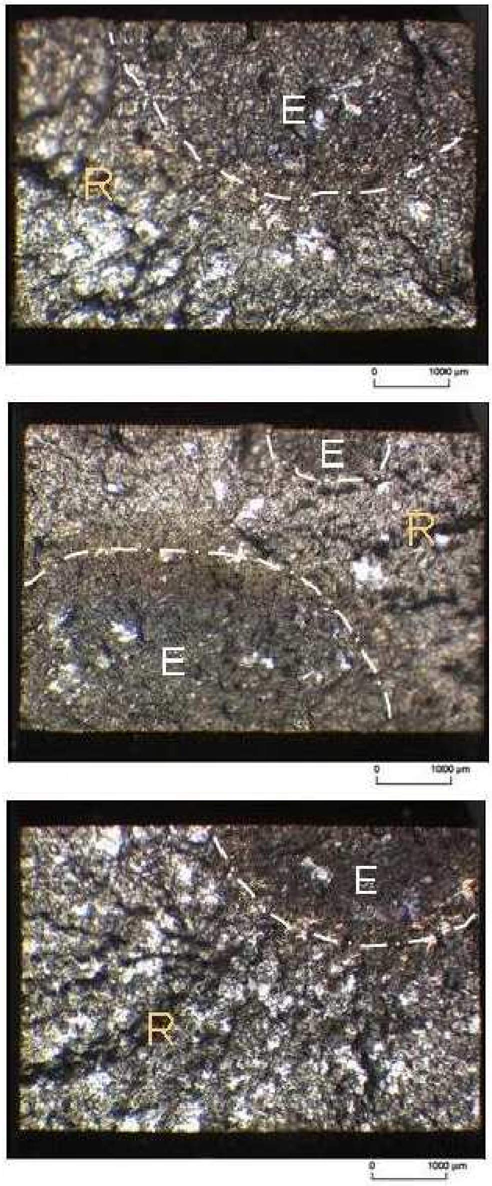

a)

b)

c)

Figure 21: Optical micrographs of fracture surfaces of notched specimens: a) specimen 1; b) specimen 2; c) specimen 3. (E) fatigue crack area, (R) final fracture area. On top and bottom of the figures is the notch base, respectively.

spheroidal void shapes and the shape evolution can be taken into account.

The TMF fatigue life model refers to the dominant damage mechanism in components of combustion engines, namely fatigue crack growth. It has a significantly lower number of adjustable parameters compared to the Sehitoglu model [26, 27], which is implemented in the software package FEMFAT HEAT (www.femfat.com). Most of the model parameters can be determined directly from isothermal stress-strain hysteresis loops.

From the theory one would expect that $A = 2\ln[a_f/a_0]/\beta \approx 8/\beta$ and $B = 1$. a_0 is the initial crack length and a_f the crack length at fracture. Indeed, for the cast iron materials considered in this paper, the exponent $B = 1$ is obtained (table 7). The measured value of A decrease with increasing fraction of graphite inclusions. In table 7, initial crack sizes are listed which are estimated from an average size of the graphite inclusions. The values of $\ln[a_f/a_0]$ are computed assuming $a_f = 2000$ μm, a typical crack length found on failed specimens. The differences in initial crack sizes cannot explain the decreasing values of A. Thus, the factor β must be variable and depend on graphite morphology and volume fraction, as it is assumed in the crack growth law for cast iron.

cast iron	A	B	a_0 in μm	$\ln[a_f/a_0]$
EN-GJS-700	25.7	1	30	4.2
EN-GJV-450	9.91	1	100	3
EN-GJL-250	2.71	1	300	1.9

Table 7: Parameters of the mechanism-based fatigue life model for different cast iron materials.

The application of the models for fatigue life prediction of the double-sided notched specimen show that the models are well applicable to engineering problems. Thus, a reduction of the number of expensive and time-consuming bench and field tests is possible.

9. Conclusions

The models for thermomechanical fatigue life prediction of cast iron, developed in Part I, are adjusted to isothermal experimental data obtained for the nodular cast iron EN-GJS-700, the vermicular cast iron EN-GJV-450 and the lamellar cast iron EN-GJL-250. Using the proposed parameter identification strategy and procedure, the adjusted model is able to predict stresses and strains and fatigue lives under non-isothermal loading conditions. The models can be applied in finite-element simulations to optimize high temperature components and, thus, to reduce the number of expensive and time-consuming bench and field tests. In a forthcoming research project, the models will be extended to account for superimposed high cycle fatigue loadings, caused by ignition pressure.

Acknowledgments

The financial support of the FVV (Research Association for Combustion Engines), Frankfurt am Main, Germany, and the technical support of the working committee under the direction of Dr. U. Schmid, MTU, Friedrichshafen, Germany, during the project no. 825 are gratefully acknowledged.

References

[1] Uihlein A, Lang KH, Seifert T, Riedel H, Mohrmann R, Maier G. TMF Lifetime Models for Cast Iron. Final report, project no. 825, FVV (Research Association for Combustion Engines), in German, 2008

[2] Chaboche JL. Time-independent constitutive theories for cyclic plasticity. Int J Plast 1986;2:149-188

[3] Chaboche JL. Constitutive equations for cyclic plasticity and cyclic viscoplasticity. Int J Plast 1989;5:247-302

[4] Chaboche JL. A review of some plasticity and viscoplasticity constitutive theories. Int J Plast 2008;24:1642-1693

[5] Gurson AL. Continuum theory of ductile rupture by void nucleation and growth- I. yield criteria and flow rules for porous ductile media. J Engr Mat Tech 1977:99;2-15

[6] Laird C, Smith GC. Crack propagation in high stress fatigue. Philosophical Magazine 1962:7;847-857

[7] Pelloux RMN. Crack extension by alternating shear. Engng Fract Mech 1970:1;697-704

[8] Schmitt W, Mohrmann R, Riedel H, Dietsche A, Fischersworring Bunk A. Modelling the fatigue life of automobile components. Fatigue 2002 - Proceedings of the Eighth International Fatigue Congress held 3 - 7 June 2002, Stockholm, Sweden (Ed. A.F. Blom), 2002;781-788

[9] Mahnken R, Stein E. Parameter identification for viscoplastic models based on analytical derivatives of a least-squares functional and stability investigations. Int J Plast 1996:12;451-479

[10] Fossum AF. Parameter estimation for an internal variable model using nonlinear optimization and analytical/numerical response sensitivities. J Eng Mater Tech 1997:119;337-345

[11] Tong J, Vermeulen B. The description of cyclic plasticity and viscoplasticity of waspaloy using unified constitutive equations. Int J Fatigue 2003:25;413-420

[12] Seifert T. Ein komplexes LCF-Versuchsprogramm zur schnellen und günstigen Werkstoffparameteridentifizierung. Proceedings 'Werkstoffprüfung 2006 - Fortschritte der Kennwertermittlung für Forschung und Praxis' (Eds. M. Borsutzki and S. Geisler), 2006;409-414

[13] Mahnken R, Stein E. A unified approach for parameter identification of inelastic material models in the frame of the finite element method. Comput Methods Appl Mech Engrg 1996:136;225-258

[14] Bruhns OT, Anding DK. On the simultaneous estimation of model parameters used in constitutive laws for inelastic material behaviour. Int J Plast 1999:15;1311-1340

[15] Kreißig R. Numerische Methoden für die Parameteridentifikation. ZAMM 1998:78;555-557

[16] Mohrmann R. Automated identification and calculation of the parameters of non-linear material models. Field Analyses for Determination of Material Parameters - Experimental und Numerical Aspects (Eds. P. Stahle and K.G. Sundin), Kluwer Academic Publisher, Dordrecht, 2003;113-122

[17] Mahnken R, Stein E. The identification of parameters for visco-plastic models via finite-element methods and gradient methods. Modelling Simul. Mater. Sci. Eng. 1994:2;597-616

[18] Scheday G, Miehe C. An unified computational framework for parameter identification of material models in finite inelasticity. PAMM 2002:1;189-190

[19] Rieger A, Scheday G, Miehe C. Parameter identification of a finite viscoplastic material model using different deterministic optimization methods. PAMM 2003:2;525-526

[20] Seifert T, Schenk T, Schmidt I. Efficient and modular algorithms in modeling finite inelastic deformations: objective integration, parameter identification and sub-stepping techniques. Comput Methods Appl Mech Eng 2007:196;2269-2283

[21] Seifert T, Schmidt I. Line-search methods in general return mapping algorithms with application to porous plasticity. Int J Numer Meth Engng 2008:73;1468-1495

[22] Luenberger DG. Linear and nonlinear programming, Second Edition, Kluwer Academic Publishers, 2003

[23] ABAQUS Theory Manual, Version 6.8, Dassault Systèmes, 2008

[24] Gologanu M, Leblond JB, Devaux J. Approximate models for ductile metals containing nonspherical voids - case of axisymmetric prolate ellipsoidal cavities. J Mech Phys Solids 1994:41;1723-1754

[25] Gologanu M, Leblond JB, Devaux J. Approximate models for ductile metals containing nonspherical voids - case of axisymmetric oblate ellipsoidal cavities. J Eng Mater Tech 1994:116;290-297

[26] Neu RW, Sehitoglu H. Thermomechanical fatigue, oxidation and creep: Part I. Damage mechanisms. Metallurgical Transactions A 1989:20A;1755-1767

[27] Neu RW, Sehitoglu H. Thermomechanical fatigue, oxidation and creep: Part II. Life prediction. Metallurgical Transactions A 1989:20A;1769-1783